




# The effect of substrate bias on the piezoelectric properties of pulse DC magnetron sputtered AlN thin films

Nguyen Quoc Khanh<sup>1,\*</sup> , János Radó<sup>1</sup>, Zsolt Endre Horváth<sup>1</sup>, Saeedeh Soleimani<sup>1</sup>, Binderiya Oyunbolor<sup>1</sup>, and János Volk<sup>1</sup>

<sup>1</sup>Centre for Energy Research, Institute of Technical Physics and Materials Science, Konkoly-Thege M. út 29-33, H-1121 Budapest, Hungary

Received: 27 July 2020

Accepted: 1 November 2020

Published online:  
13 November 2020

© The Author(s) 2020

## ABSTRACT

Substrate bias was applied for AlN deposition on rolled Ni sheet during pulse DC reactive sputtering to overcome the difficulty caused by thermal expansion mismatch between Ni substrate and AlN upon substrate heating. It was shown by Piezoresponse Force Microscopy (PFM) that the quality of the deposited AlN layer depends strongly on the negative substrate bias, i.e., the energy transferred via the bombardment of the accelerated positive ions on the sample. As the negative substrate bias becomes larger, the so formed layer shows higher piezoresponse, and better homogeneity. A Z-cut LiNbO<sub>3</sub> single crystal was used as a reference to correct the PFM signals. The highest average  $d_{33}$  piezoelectric coefficient value, achieved at  $-100$  V substrate bias, is  $3.4$  pm/V indicating the feasibility of AlN deposition on rolled Ni substrate for vibration energy harvesting applications.

## 1 Introduction

Tremendous number of sensors to be applied nowadays over the world necessitates the use of sustainable, maintenance-free, and self-powered sensor system [1]. Piezoelectric materials are promising for such purpose, being a good transducer to convert directly the stimulus into electric signal in the case of sensing, or into electrical energy as vibrational energy harvesters for sensor operation.

Aluminum nitride (AlN) thin film has been widely studied for piezoelectric energy harvester

application, among others, due to its excellent properties, like piezoelectricity even at high temperature, extreme hardness, good thermal and chemical stabilities, and not least, environment friendly lead-free material. [2]. AlN films can be grown by various methods including Chemical Vapor Deposition (CVD) [3], MetalOrganic Chemical Vapor Deposition (MOCVD) [4], Molecular Beam Epitaxy (MBE) [5], Pulsed Laser Deposition (PLD) [6], and Atomic Layer Deposition (ALD) [7]. However, these methods are expensive, and high processing temperatures are required. Direct Current (DC) and Radio Frequency

Address correspondence to E-mail: [khanh@mfa.kfki.hu](mailto:khanh@mfa.kfki.hu)

(RF) reactive ion sputtering, being low temperature and low-cost processes with excellent reproducibility and high output, therefore, are the most frequently applied techniques to produce AlN thin layer [8–10].

Silicon wafer (with or without top oxide) is the most commonly used substrate for AlN deposition. Depending on requirements of the device to be fabricated different metals are deposited as buried electrode prior to AlN growth [11–14]. Sometimes sapphire or glass substrate have been also used [15, 16]. Common character of these substrates is their smooth surface, which is indispensable for certain applications, like Surface Acoustic Wave Sensor (SAWS) [12, 17], and Film Bulk Acoustic Resonators (FBAR) [9]. It is a consensus among researchers that the character of the substrate surface has a role as important as the deposition conditions on the properties of the AlN crystal grown on it, that is substrate crystal lattice and surface morphology all affect the (002) preferential growth of AlN film [11, 13, 14].

In a few MEMS applications metal substrate is a viable alternative of Si where the high fracture toughness, low substrate and micromachining costs are concerned. For example, unimorph piezoelectric energy harvesters, which convert mechanical energy into electricity, require a relatively large area, high mechanically robustness therefore laser cut metal film, such as stainless steel [18] or Ni is a reasonable choice. Generally, a substrate heating of c.a. 500 °C is applied during the growth of AlN to improve its crystal quality *via* enhancing the surface diffusion [9, 16, 19, 20]. However, in the case of Ni sheet, the substrate heating is not applicable due to the high difference of thermal expansion coefficient between Ni substrate ( $13 \times 10^{-6} \text{ K}^{-1}$ ) [21] and AlN ( $4.2 \times 10^{-6} \text{ K}^{-1}$ ) [22]. So one can expect that as the sample cools down from high temperature after deposition, the adhesion between AlN layer and Ni substrate can degrade significantly, even AlN layer can detach from Ni substrate, which makes the application of such structure for vibration energy harvester impossible. For this reason, we have applied the new approach, namely the negative bias on Ni substrate during deposition of AlN layer at room temperature. The substrate bias can affect the quality of deposited layer via the impact of the energetic ions on the sample surface [16, 23–25]. By increasing the energy supplied to the film the surface diffusion can be enhanced, leading to an increase in the mean distance which the adatoms can travel, reaching the lowest

energy sites [26], thus results in an improved crystal growth. In return, one may expect the resputtering at the substrate, which may decrease the rate of the AlN layer deposition.

Though the piezoelectric coefficient can be measured by macroscopic techniques, like Berlincourt Piezometer [27], series capacitance [28], interferometer [29], but characterization in nanoscale (electromechanical displacement variation, polarity) using Piezoresponse Force Microscopy (PFM) [30, 31] helps to understand better the influence of deposition parameters on piezoelectric properties of the deposited AlN layer, and so to optimize the parameters of the deposition process. In PFM measurement, contact resonance could be applied to enhance the sensitivity. However, delicate techniques are needed to handle the problem of contact resonance shift caused by the surface morphology, like Dual-Frequency Resonance-Tracking (DFRT) PFM [32], or Band-Excitation (BE) PFM [33]. Furthermore, model calculations are needed to make correction on the results [34, 35]. In lack of the listed techniques, off-resonant measurement is a reasonable choice; however, one should take into account that the signal-to-noise ratio is deteriorated, and the electrostatic effect is still to be considered in this case. The latter one could be essential in the PFM signal, hence make such measurement unreliable. Therefore, elimination of the electrostatic contribution is vital point in PFM measurement.

In this report we used PFM and X-Ray Diffractometry (XRD) techniques to investigate the effect of substrate bias on the quality of AlN layer first time deposited at RT on 80 µm thick rolled Ni sheet which is ready to use as the active element of the flexible energy harvester. A Z-cut LiNbO<sub>3</sub> crystal (z-LN) having well-known piezocoefficients has been used as a reference for the correction of PFM results.

## 2 Experimental

### 2.1 Sample preparation

Rolled Ni sheets with thickness of 80 µm have been ultrasonically cleaned stepwise in acetone, ethanol, deionized water for 5 min, and purged in nitrogen. Then the sample was loaded into the chamber of the pulse DC magnetron sputtering system (VAKSIS-MiDAS). The base pressure was in the range of  $3\text{--}6 \times 10^{-8}$  Torr. The substrate was further cleaned by 30 W

Ar plasma for 10 min. Then AlN films were deposited onto Ni substrates by reactive sputtering with constant parameters except for deposition time and substrate bias voltage. The sputtering cathode was thick pure Al target (99.999%) and was continuously water cooled. The gases used are high-purity argon (99.999%) as the working gas and nitrogen (99.999%) as reactive gas. During deposition total pressure was 5 mTorr, and no intentional heating was applied, the estimated substrate temperature due to plasma heating is around 100 °C. The detailed deposition conditions are listed in Table 1.

## 2.2 Characterization

Atomic Force Microscopy (AIST NT smart-SPM1000) was used to study the morphology of the films in semi-contact mode, as well as piezoelectric properties of AlN layer in top-PFM mode, i.e., the probe movement between scan raster points is performed in semi-contact mode, while PFM measurement is carried out in the raster points using contact mode technique. This hybrid operation mode enables the use of stiff cantilever for PFM scan. For studying the electrostatic effect, at first three kinds of tips with 0.2, 3, 42 N/m spring constant were compared on thick SiO<sub>2</sub> thermally grown on p-silicon sample with thickness of 1.3 μm like that of AlN films, where the bottom electrode was 100 nm Al sintered in forming gas for 30 min to achieve ohmic contact with p-Si. Later on, for the actual PFM tests a conductive probe with spring constant of 42 N/m was used (PPP-NCHPt, Nanosensors). The pressing force to the tip was kept at 120 nN for contact mode. The amplitude and frequency of the exciting  $V_{ac}$  were in the range of 0–9 V and 51 kHz, respectively. However,  $V_{ac}$  up to 4 V was applied in most case to avoid the fast

degradation of the tip according to our PFM experience. The measured data have been evaluated by Gwyddion software package [36]. For comparison, the samples were also measured by Berlincourt piezometer (Piezotest PM300) using 10.4 N static force (preload), and 0.25 N dynamic force at 110 Hz frequency.

To investigate the structure of the obtained films, a Bruker AXS D8 Discover diffractometer was used in Bragg-Brentano geometry ( $\theta$ – $2\theta$  geometry), at room temperature; with Cu K $\alpha$  radiation. The XRD diffractograms were obtained at scanned angle of  $2\theta$  varying from 30 to 70°. The film thicknesses were measured by Scanning Electron Microscope (SEM) at the cross-section of the cleaved sample.

## 3 Results and discussion

### 3.1 Surface morphology of the films

Ni substrate, being rolled sheet, has a wavy feature with height fluctuates within few hundred nanometers (Fig. 1a). It is clear that the surface roughness on large area is dominated by the substrate. Therefore, the roughness of the AlN layer is only correctly measured on the area with dimension of c.a. 1 μm, where the substrate is relatively flat. For this reason, both AFM, and PFM have been carried out on sample area of 1 × 1 μm<sup>2</sup>.

Figure 1b–e shows the AFM height images of the AlN layers deposited with different bias voltages, from which the grain size and surface roughness (in RMS) were determined. The in-plane grain size was characterized by equivalent disk radius using the watershed algorithm in Gwyddion. Because of small scanned area, the size distributions are somewhat scattered. The mean grain size increases slightly with increasing bias voltage from ca. 28 nm for unbiased sample to 46 nm for – 100 V bias (Fig. 1f). The surface roughness, however, remains around 14 nm for all applied bias voltage. Deposition rate was determined using the thickness measured by SEM on the cross-section of the samples, and deposition time. The deposition rate decreases from 13.4 to 10.4 nm/min as the bias voltage increases from 0 to – 70 V, then increases to 14.6 nm/min. for – 100 V substrate bias. The rates are acceptable in all cases indicating that the resputtering is tolerable in the range of applied substrate bias. Deposition rate also seems to

**Table 1** Sputtering conditions for the deposition of AlN films

Target	Pure aluminum (3 inch, 99.999%)
Target-substrate distance	13 cm
Base pressure	$3.0 \times 10^{-8}$ Torr
Ar/N <sub>2</sub> gas flow rates	80/20 sccm
Working gas pressure	5 mTorr
Sputtering power	370 W
Deposition time	90–120 min
Bias substrate	0, – 50, – 70 and – 100 V
Substrate temperature	~ 100 °C (plasma heating)

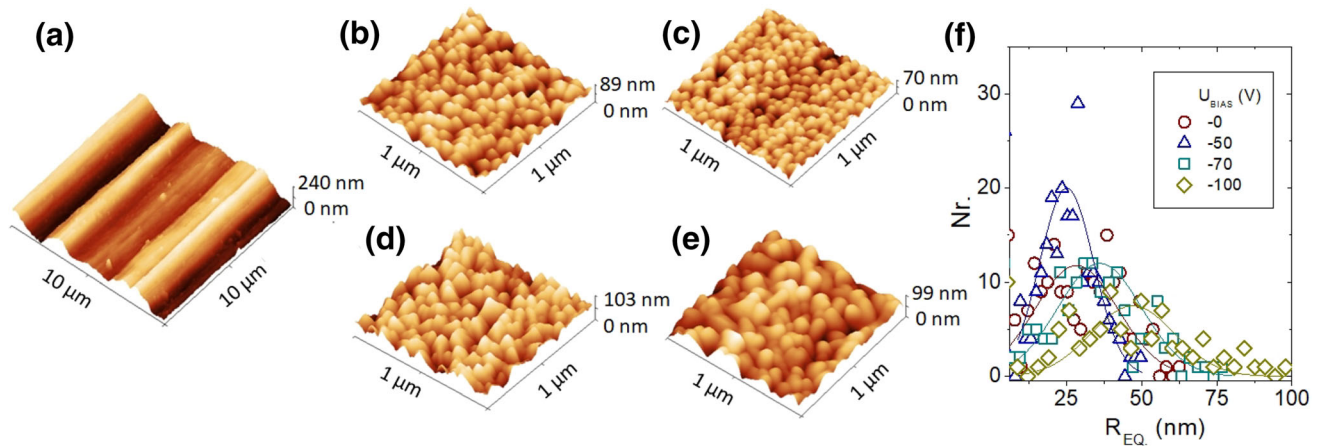


**Fig. 1** AFM height image of rolled Ni substrate (a), small area scan on the AlN layer deposited with  $V_{\text{bias}}$  of 0V (b), - 50 V (c), - 70 V (d), - 100 V (e) and the corresponding grain size distributions (f)

change oppositely compared to the surface roughness for different substrate bias; the higher the deposition rate the smoother the surface is.

### 3.2 The effect of the cantilever stiffness

Together with the electromechanical displacement ( $D_{\text{EM}}$ ) the utmost non-piezoelectric contribution to the displacement ( $D_{\text{PR}}$ ) measured by PFM is caused by the electrostatic force between sample and tip, as well as sample and cantilever. Practically the electrostatic part is handled as the first harmonic of the cantilever oscillation due to alternating excitation voltage [37, 38]

$$D_{\omega,ES} = k^{-1} \frac{dC}{dz} (V_{dc} + V_{CPD}) V_{ac} \sin(\omega t)$$

where  $D_{\omega,ES}$  is the electrostatic displacement,  $k$ ,  $C$ ,  $V_{dc}$ ,  $V_{CPD}$ , and  $V_{ac} \sin(\omega t)$  are the spring constant, contact capacitance, optional DC voltage, contact potential difference, and AC voltage, respectively.

From the equation above one can see that the effect of the electrostatic force can be eliminated by application of proper  $V_{dc}$ , or by the use of a stiff cantilever. We used a 1.3  $\mu\text{m}$  thick oxide thermally grown on p-silicon, i.e., non-piezoelectric sample to show the benefit of stiff cantilever. Figure 2 shows the displacement measured using cantilevers with different spring constants as a function of  $V_{ac}$ . Since  $V_{dc}$  cannot be set in our scanning probe system, only  $V_{ac}$  was applied. For each  $V_{ac}$  bias 100 acquisitions with 100 ms acquisition time were recorded at the same position of the sample surface. Because of the smooth surface and excellent homogeneity of the  $\text{SiO}_2$  thin

films no area averaging was needed, in contrast to the polycrystalline AlN films.

As one can see in Fig. 2, the effect of electrostatic force decreases as the stiffness of the probe cantilever increases. For the stiffest cantilever of 42 N/m, the electrostatic contribution, which could cause a significant error in the piezoelectric properties determined from the measured data, is practically eliminated.

### 3.3 Piezoelectric response

Figure 3 shows the amplitude map measured by PFM at  $V_{ac} = 4$  V for AlN films sputtered at different bias voltages ( $V_{\text{bias}}$ ). The sample sputtered under zero bias shows very weak piezoresponse indicating a

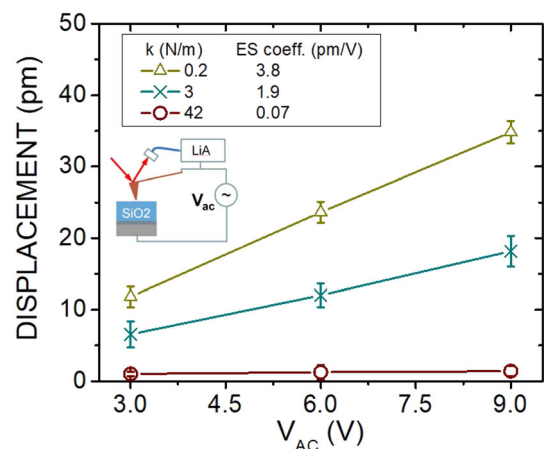


**Fig. 2** PFM displacement responses due to electrostatic force on non-piezoelectric  $\text{SiO}_2$  blank sample. The electrostatic coefficients also shown in the legend



poor crystal quality, or crystal growth in inferior direction. There are few small areas showing electromechanical (EM) displacement around 1–2 pm over background for  $V_{ac} = 4$  V. The major part of the image equal to the background level determined by fitting the piezoresponses at different  $V_{ac}$ , i.e., the intersection of fitting line with the displacement ( $y$ ) axis. Such dead zones (DZ) are marked by dark cyan in Fig. 3. The ratio of dead zones decreases as bias voltage gets larger. Practically no DZ is found on sample biased with  $-100$  V. Also, the EM displacement outside DZs shows higher value as larger substrate bias was applied. The attenuation of dead zone and the increasing in displacement both reveal the benefit of applying substrate bias.

The distribution of PFM response gives information on the homogeneity of the layer. The narrower the distribution, the more homogeneous the layer is. In the present case the phase output of the lock-in amplifier was manually shifted to 0 to ease the comparison (Fig. 4b). The  $y$ -axis represents the probability density function for which the integration over the entire displacement space equals to 1. The amplitude distribution of unbiased sample is at the background level, while its phase distribution is extremely wide. As bias voltage increases, the layer becomes more and more homogeneous, i.e., the phase distribution is narrower and higher. Though

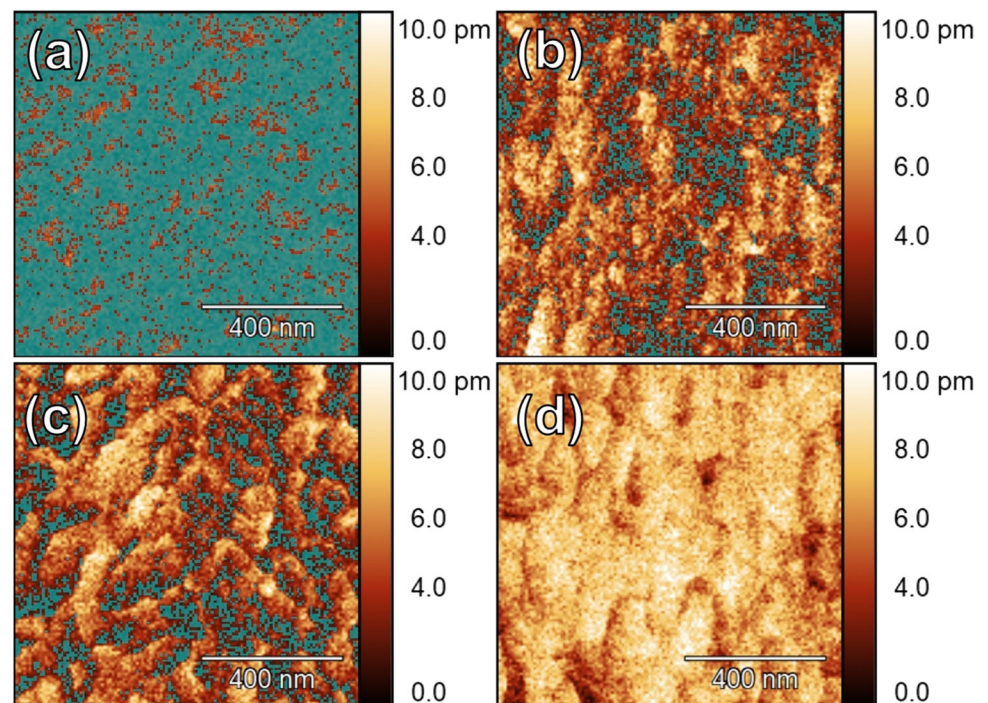
the displacement distribution peak of unbiased sample is narrow, and high, it is due to the fact that it contains mainly the background. Interestingly, increasing substrate bias from 50 to 70 V has almost no effect on the amplitude and phase distribution. For the best sample ( $V_{bias} = -100$  V) the mean displacement is c.a. 6.5 pm at  $V_{AC} = 4$  V, and the FWHM of phase distribution is about  $22^\circ$ .

For the determination of the effective piezoelectric coefficient, one should measure the EM displacement at different exciting AC voltage to eliminate the background. Figure 5 presents the measured displacement as a function of  $V_{ac}$ . Each point is the average of a  $128 \times 128$  point scan over  $1 \times 1 \mu\text{m}^2$  area of the samples. The slope of the displacement-voltage fitting line gives the effective EM coefficient. The highest effective coefficient of 1.59 pm/V achieved at  $V_{bias} = -100$  V bias is rather small compared to the value of 5.6 pm/V for bulk AlN.[39]

### 3.4 Correction of the PFM data

The measured effective coefficients are well below the intrinsic value. One reason of low measured value can be the clamp effect, that is the thin layer to be measured is not under free boundary condition, but it is clamped to the substrate. Therefore, the measured effective piezoelectric coefficient  $d_{33\text{eff}}$  of thin layer

**Fig. 3** Piezoresponse amplitude image of AlN layers deposited with  $V_{bias} = -0$  V (a),  $-50$  V (b),  $-70$  V (c),  $-100$  V (d). PFM carried out with  $V_{ac} = 4$  V. Area with background equivalent displacement marked by dark cyan



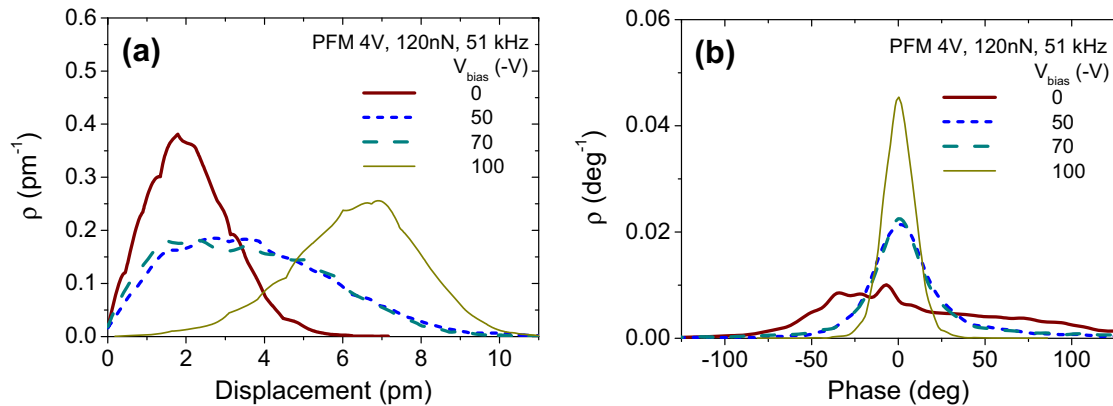


**Fig. 4** Amplitude (a) and phase (b) distribution of samples deposited at various substrate bias voltage

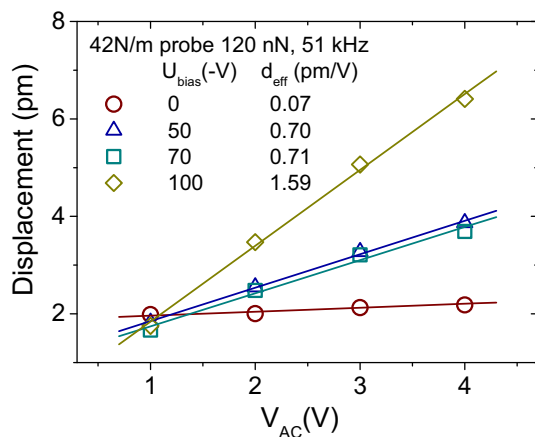


**Fig. 5** Displacements as a function of exciting  $V_{\text{ac}}$  for AlN layers deposited with different bias voltages. Lines are the linear fits; their slope gives the effective piezoelectric coefficients shown in the legend

can be related to the unclamped one  $d_{33}$  by the following relationship [40]:

$$d_{33,\text{unclamp}} = d_{33,\text{eff}} (S_{11}^E + S_{12}^E) / (S_{11}^E + S_{12}^E + S_{13}^E)$$

Using  $S_{11}^E = 3$ ,  $S_{12}^E = -0.9$ ,  $S_{13}^E = -0.6 \text{ TPa}^{-1}$  [41] the clamp effect correction factor is  $C_{\text{clamp}} = 1.4$ .

The second origin of the underestimated piezoelectric coefficient is the tip-shape effect, i.e., the electrostatic field below the sharp tip is not homogenous and depends on the radius of the tip, in contrast to the macroscopic piezometer technique which can be described by a parallel plate capacitor model. To correct this effect, a second correction was performed using a Z-cut LiNbO<sub>3</sub> single crystal (z-LN) reference with a thickness of c.a. 300  $\mu\text{m}$ . The displacement of z-LN surface as a function of exciting  $V_{\text{ac}}$  is presented

in Fig. 6, from which the effective coefficient obtained by linear fitting is 4.1 pm/V which is smaller compared to the intrinsic one of z-LN (6.2 pm/V) [42]. We note that the clamp effect mentioned above is not the case here, because the crystal is much thicker than the thickness limit of the layer, within which the clamp effect is valid [29]. Taking into account the clamp effect and the calibration on z-LN a consolidated correction factor of  $C_{\text{cons}} = 6.2/4.1 \times C_{\text{clamp}} = 2.12$  was calculated.

$$d_{33} = C_{\text{cons}} \times d_{33,\text{eff}}$$

Using  $C_{\text{cons}}$  correction factor, the best average value obtained by substrate bias of  $-100 \text{ V}$  is 3.4 pm/V. The map of the local  $d_{33}$  that is the corrected  $d_{33}$  distribution in nanoscale of the AlN films can be obtained using the linear fit of corresponding points of the displacement data sets measured at different

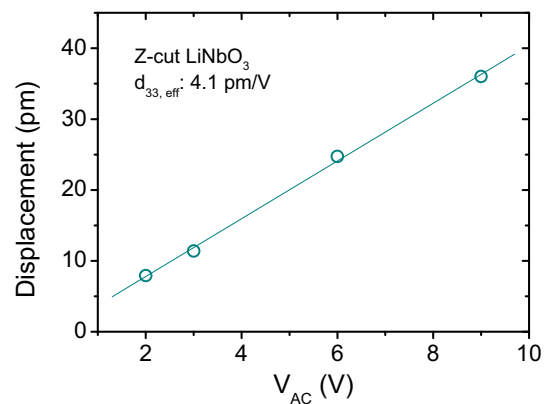


**Fig. 6** Displacements as a function of exciting  $V_{\text{ac}}$  for 300  $\mu\text{m}$  thick Z-cut LiNbO<sub>3</sub> single crystal. The slope of the linear fit gives the effective piezoelectric coefficient shown in the legend

exciting  $V_{ac}$ . Figure 7 presents the corrected  $d_{33}$  map of AlN film deposited with  $-100$  V bias, together with the line-cut indicated by white line in Fig. 7a. One can observe in Fig 7b that in some regions the obtained  $d_{33}$  data approach the bulk AlN value of  $5.6$  pm/V [39]. This finding is probably the manifestation of (002) preferential growth.

The corrected average piezoelectric coefficient, DZ ratio, deposition rate, grain size (EDR), and surface roughness (RMS) as a function of applied substrate bias are summarized in Fig. 8. The increasing tendency of grain size with bias may be associated with the increasing energy transferred by the bombardment to the adatoms on the sample surface, which results in larger surface diffusion length, thus larger grain size. However, the reason of the change in deposition rate is still unclear. For comparison, the piezoelectric coefficients measured by Berlincourt method are also presented in Fig. 8e. We note that Si also has been used as substrate in the case of  $-100$  V bias. The values measured by Berlincourt method on Ni, and Si substrate are  $2.42$ , and  $1.2$  pC/N, respectively, which shows the superiority of Ni substrate. As shown by Fig. 8, the  $-100$  V bias voltage is proved to be the best value, which

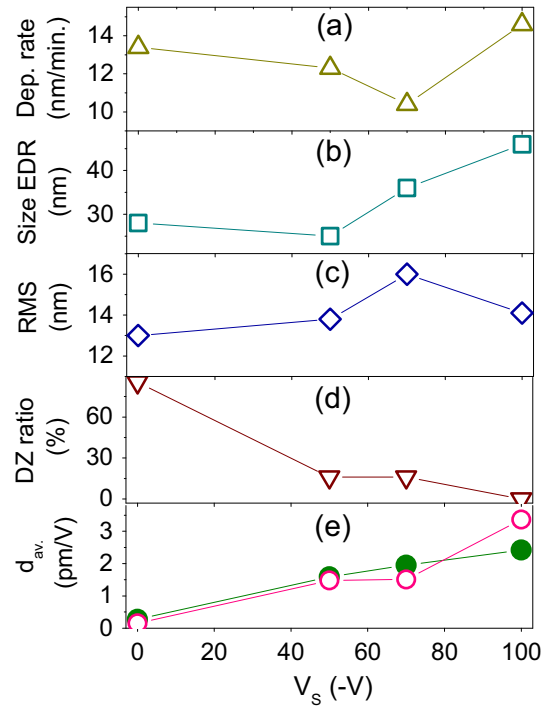


**Fig. 8** Deposition rate (a), grain size (equivalent disk radius) (b), surface roughness (RMS) (c), dead zone ratio (d), and corrected average piezoelectric coefficient (e) as a function of substrate bias voltage. Piezoelectric coefficient measured by macroscopic method (Piezometer) also shown in (e) for comparison (green dots)

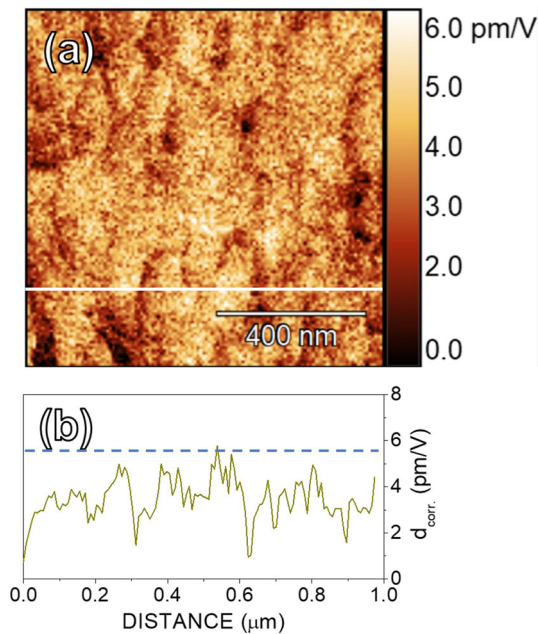


**Fig. 7** Corrected  $d_{33}$  map of AlN film deposited at  $-100$  V substrate bias (a), and a characteristic line-cut (b) along the white line. Dashed line indicates the  $d_{33}$  piezoelectric coefficient of bulk AlN

produced the highest effective coefficient with high deposition rate, and large grain size. There is a fair matching between PFM and piezometer results indicating that using proper probe and correction on reference sample, PFM can be a suitable tool for the investigation of piezoelectric materials in nanoscale.

### 3.5 Texture of the films

As mentioned in the introduction section, the energy deposition via the impact of the charged particles accelerated by the electric field of the substrate bias on the sample surface promotes the adatom mobility, which can moves to the lowest energy sites to build in. In the case of unbiased sample, however, the kinetic energy of sputtered particles is low, because they have collided once or more times on other particles in plasma due to long target to substrate distance in our case. What is more, a high number of AlN dimers can be formed via collisions in plasma

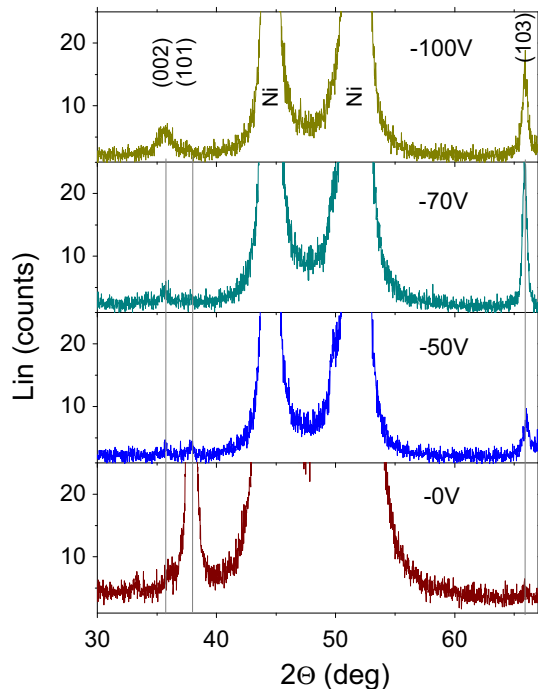


**Fig. 9** XRD patterns of AlN films deposited using different substrate bias

with the bond similar to one kind (B1 bond) of those linking the (101) planes [43, 44]. Both low surface mobility as well as formation of AlN dimers are favored for growth in [101] direction as shown by XRD in Fig. 9. The (101) plane is semipolar, and its quality in the present case may be low due to low surface mobility of adatoms. Therefore, the piezoresponse of AlN layer is inferior, as shown by PFM (Fig. 3). As the bias voltage increases, the enhanced surface diffusion promotes the formation of smaller energy bonds (B2), thus initiates the growth of (103) and (002) plans, which have low surface energy. The higher surface mobility also promotes the formation of larger grain, smoother surface. According to XRD scans (Fig. 9), the dominating texture for all AlN layer deposited with substrate bias is (103) plane, which is about 12 degrees off to the (002) one in AlN single crystal structure, so-called semipolar crystallographic plane. The growth of (103) and (002) contributes to the improvement of the piezoelectric properties of AlN layer. However, the dominating presence of semipolar (103) plane, and the possibility of defects created by ion bombardment may cause the low effective piezoelectric efficient compared to bulk value.

## 4 Conclusion

The effect of substrate bias during sputtering deposition of AlN layers on rolled Ni sheets has been investigated by means of semi-contact AFM and contact PFM modes. Using non-piezoelectric SiO<sub>2</sub> sample the probe with high cantilever spring constant (42 N/m) was demonstrated to eliminate the contribution of electrostatic force in piezoelectric response, thus making the PFM results reliable. It has been shown that, without proper energy supply ( $V_{\text{bias}} = 0\text{V}$ ), the layer consists mostly of dead zones, whose piezoresponse is the same like the background level determined by fitting the piezoresponse at various  $V_{\text{ac}}$  values. The ratio of the dead zone decreases and the homogeneity of the piezoresponse is better as the supplied energy via substrate bias increases indicating a crystal growth in a better preferential direction, which was confirmed by XRD results. As a consequence, the effective piezoelectric coefficient measured on the layer increases. Using Z-cut LiNbO<sub>3</sub> single crystal as a reference a correction factor of 2.12 was calculated. The corrected average values are in fair agreement with that measured by macroscopic method (Piezometer). The obtained high spatial resolution  $d_{33}$  map proves that using a proper probe and correction on a reference sample off-resonant PFM technique is a powerful quantitative technique for the investigation of piezoelectric materials in nanoscale. The best average coefficient value achieved at -100V substrate bias is 3.3 pm/V indicating the feasibility of substrate bias assisted AlN deposition on rolled Ni sheet for vibrational energy harvesting applications.

## Acknowledgements

This work was supported by the National Research, Development and Innovation Fund of the Hungarian Government in the framework of KoFAH, NVKP\_16-1-2016-0018. The authors thank Levente Illés for thickness measurement by SEM, and Erika Tunyogi for assistance in PFM evaluation. J. R. acknowledges the support of the New National Excellence Program of the Ministry for Innovation and Technology, ÚNKP-19-3-III-OE-51.

**Open Access** This article is licensed under a Creative Commons Attribution 4.0 International License, which permits use, sharing, adaptation, distribution



and reproduction in any medium or format, as long as you give appropriate credit to the original author(s) and the source, provide a link to the Creative Commons licence, and indicate if changes were made. The images or other third party material in this article are included in the article's Creative Commons licence, unless indicated otherwise in a credit line to the material. If material is not included in the article's Creative Commons licence and your intended use is not permitted by statutory regulation or exceeds the permitted use, you will need to obtain permission directly from the copyright holder. To view a copy of this licence, visit <http://creativecommons.org/licenses/by/4.0/>.

## Funding

Open access funding provided by ELKH Wigner Research Centre for Physics..

## References

1. F. Narita, M. Fox, A review on piezoelectric, magnetostrictive, and magnetoelectric materials and device technologies for energy harvesting applications. *Adv Eng. Mater.* (2017). <https://doi.org/10.1002/adem.201700743>
2. V. Mortet, M. Nesladek, K. Haenen, A. Morel, M. D'Olielaeager, M. Vanecek, Physical properties of polycrystalline aluminium nitride films deposited by magnetron sputtering. *Diamond Relat. Mater.* **13**, 1120 (2004). <https://doi.org/10.1016/j.diamond.2003.10.082>
3. R. Rodriguez-Clemente, B. Aspar, N. Azema, B. Armas, C. Combescure, J. Durand, A. Figueras, Morphological properties of chemical vapour deposited AlN films. *J. Cryst. Growth* **133**, 59 (1993). [https://doi.org/10.1016/0022-0248\(93\)90103-4](https://doi.org/10.1016/0022-0248(93)90103-4)
4. A. Kakanakova-Georgieva, D. Nilsson, E. Janze, High-quality AlN layers grown by hot-wall MOCVD at reduced temperatures. *J. Cryst. Growth* **338**, 52 (2012). <https://doi.org/10.1016/j.jcrysgro.2011.10.052>
5. S. Karmann, H.P.D. Schenk, U. Kaiser, A. Fissel, Wo. Richter, Growth of columnar aluminum nitride layers on Si(111) by molecular beam epitaxy. *Mater. Sci. Eng. B* **50**(1–3), 228–231 (1997). [https://doi.org/10.1016/S0921-5107\(97\)00168-2](https://doi.org/10.1016/S0921-5107(97)00168-2)
6. P. Verardi, M. Dinescu, C. Gerardi, L. Mirengi, V. Sandu, AlN thin films deposition by laser ablation of Al target in nitrogen reactive atmosphere. *Appl. Surf. Sci.* **109–110**, 371–375 (1997). [https://doi.org/10.1016/S0169-4332\(96\)00751-9](https://doi.org/10.1016/S0169-4332(96)00751-9)
7. M. Alevli, C. Ozgit, I. Donmez, N. Biyikli, Structural properties of AlN films deposited by plasma-enhanced atomic layer deposition at different growth temperatures. *Phys. Stat. Sol. A* **209**(2), 266 (2012). <https://doi.org/10.1002/pssa.201127430>
8. G.F. Iriarte, J.G. Rodríguez, F. Calle, Synthesis of c-axis oriented AlN thin films on different substrates: A review. *Mater. Res. Bull.* **45**, 1039 (2010). <https://doi.org/10.1016/j.materresbull.2010.05.035>
9. H. Jin, B. Feng, S. Dong, C. Zhou, J. Zhou, Y. Yang, T. Ren, J. Luo, D. Wang, Influence of substrate temperature on structural properties and deposition rate of AlN thin film deposited by reactive magnetron sputtering. *J. Elect. Mater.* **41**, 1948 (2012). <https://doi.org/10.1007/s11664-012-1999-4>
10. A. Kale, R.S. Brusa, A. Miotello, Structural and electrical properties of AlN films deposited using reactive RF magnetron sputtering for solar concentrator application. *Appl. Surf. Sci.* **258**, 3450 (2012). <https://doi.org/10.1016/j.apsusc.2011.11.095>
11. M. Akiyama, K. Nagao, N. Ueno, H. Tateyama, T. Yamada, Influence of metal electrodes on crystal orientation of aluminum nitride thin films. *Vacuum* **74**, 699 (2004). <https://doi.org/10.1016/j.vacuum.2004.01.052>
12. M. Clement, L. Vergara, J. Sangrador, E. Iborra, A. Sanz-Hervás, SAW characteristics of AlN films sputtered on silicon substrates. *Ultrasonics* **42**, 403 (2004). <https://doi.org/10.1016/j.ultras.2004.01.034>
13. G.F. Iriarte, J. Bjurström, J. Westlinder, F. Engelmark, I.V. Katardjiev, Synthesis of C-axis-oriented AlN thin films on high-conducting layers: Al, Mo, Ti, TiN, and Ni. *IEEE Trans. Ultra. Ferro. Freq. Cont.* **52**, 1170 (2005)
14. A. Sanz-Hervás, L. Vergara, J. Olivares, E. Iborra, Y. Morilla, J. García-López, M. Clement, J. Sangrador, M.A. Respaldiza, *Diamond & Related Mater.* **14**, 1198 (2005). <https://doi.org/10.1016/j.diamond.2004.11.010>
15. L. Monteagudo-Lerma, S. Valdeza-Felip, A. Núñez-Cascajero, M. González-Herráez, E. Monroy, F.B. Naranjo, Two-step method for the deposition of AlN by radio frequency sputtering. *Thin Solid Films* **545**, 149 (2013). <https://doi.org/10.1016/j.tsf.2013.07.062>
16. J. Wang, Q. Zhang, G.F. Yang, C.J. Yao, Y.J. Li, R. Sun, J.L. Zhao, S.M. Gao, Effect of substrate temperature and bias voltage on the properties in DC magnetron sputtered AlN films on glass substrates. *J. Mater. Sci: Mater. Electron.* (2015). <https://doi.org/10.1007/s10854-015-4125-6>
17. F. Wang, F. Xiao, D. Song, L. Qian, Y. Feng, B. Fu, K. Dong, C. Li, K. Zhang, Research of micro area piezoelectric properties of AlN films and fabrication of high frequency SAW

- devices. *Microelect. Eng.* **199**, 63 (2018). <https://doi.org/10.1016/j.mee.2018.07.016>
18. I. Kanno, Piezoelectric MEMS for energy harvesting. *J. Phys.: Conf. Series* **660**, 012001 (2015). <https://doi.org/10.1088/1742-6596/660/1/012001>
19. J. Yang, X. Jiao, R. Zhang, H. Zhong, Y. Shi, B. Du, Growth of AlN films as a function of temperature on Mo films deposited by different techniques. *J. Elect. Mater.* **43**, 369 (2014). <https://doi.org/10.1007/s11664-013-2867-6>
20. F. Medjani, R. Sanjinés, G. Allidi, A. Karimi, Effect of substrate temperature and bias voltage on the crystallite orientation in RF magnetron sputtered AlN thin films. *Thin Solid Films* **515**, 260 (2006). <https://doi.org/10.1016/j.tsf.2005.12.145>
21. R.E. Taylor, CINDAS Data Series on Materials Properties, Thermal Expansion of Solids, Vol 1–4, ASM Int. (1998)
22. G.A. Slack, S.F. Bartram, Thermal expansion of some diamondlike crystals. *J. Appl. Phys.* **46**, 89–98 (1975). <https://doi.org/10.1063/1.321373>
23. A.K. Chu, C.H. Chao, F.Z. Lee, H.L. Huang, Influences of bias voltage on the crystallographic orientation of AlN thin films prepared by long-distance magnetron sputtering. *Thin Solid Films* **429**, 1 (2003). [https://doi.org/10.1016/S0040-6090\(02\)01286-5](https://doi.org/10.1016/S0040-6090(02)01286-5)
24. H. Suharyadi, The influence of substrate bias and sputtering pressure on the deposited aluminium nitride for magnetoelectric sensors. *J. Phys.: Conf. Series* **1517**, 012104 (2020). <https://doi.org/10.1088/1742-6596/1517/1/012104>
25. C.S. Sandu, F. Parsapour, D. Xiao, R. Nigon, L.M. Riemer, T. LaGrange, P. Murali, Impact of negative bias on the piezoelectric properties through the incidence of abnormal oriented grains in Al<sub>0.62</sub>Sc<sub>0.38</sub>N thin films. *Thin Sol. Film* **697**, 137819 (2020). <https://doi.org/10.1016/j.tsf.2020.137819>
26. M. Ohring, *The Materials Science of Thin Films* (Academic Press Inc, San Diego, California, 1992)
27. D. Berlincourt, H. Jaffe, Elastic and piezoelectric coefficients of single-crystal barium titanate. *Phys. Rev.* **111**, 143 (1958). <https://doi.org/10.1103/PhysRev.111.143>
28. M. Al Ahmad, R. Plana, Piezoelectric coefficients of thin film aluminum nitride characterizations using capacitance measurements. *IEEE Microw. Wirel. Compon. Lett.* **19**, 140 (2009). <https://doi.org/10.1109/LMWC.2009.2013682>
29. A. Ababneh, U. Schmid, J. Hernando, J.L. Sánchez-Rojas, H. Seidela, The influence of sputter deposition parameters on piezoelectric and mechanical properties of AlN thin films. *Mater. Sci. Eng. B* **172**, 25 (2010). <https://doi.org/10.1016/j.mseb.2010.05.026>
30. T. Kamohara, M. Akiyama, N. Kuwano, Influence of polar distribution on piezoelectric response of aluminum nitride thin films. *Appl. Phys. Lett.* **92**, 093506 (2008). <https://doi.org/10.1063/1.2892041>
31. M. Reusch, K. Holc, W. Pletschen, L. Kirste, A. Žukauskaitė, T. Yoshikawa, D. Iankov, O. Ambacher, V. Lebedev, Analysis and optimization of sputter deposited AlN-layers for flexural plate wave devices. *J. Vac. Sci. Technol. B* **34**, 052001 (2016). <https://doi.org/10.1116/1.4959580>
32. B.J. Rodriguez, C. Callahan, S.V. Kalinin, R. Proksch, Dual-frequency resonance-tracking atomic force microscopy. *Nanotechnology* **18**, 475504 (2007). <https://doi.org/10.1088/0957-4484/18/47/475504>
33. S. Jesse, S.V. Kalinin, R. Proksch, A.P. Baddorf, B.J. Rodriguez, The band excitation method in scanning probe microscopy for rapid mapping of energy dissipation on the nanoscale. *Nanotechnology* **18**, 435503 (2007). <https://doi.org/10.1088/0957-4484/18/43/435503>
34. S.V. Kalinin, B.J. Rodriguez, S. Jesse, K. Seal, R. Proksch, S. Hohlbauch, I. Revenko, G.L. Thompson, A.A. Vertegel, Towards local electromechanical probing of cellular and biomolecular systems in a liquid environment. *Nanotechnology* **18**, 424020 (2007). <https://doi.org/10.1088/0957-4484/18/42/424020>
35. N. Balke, S. Jesse, P. Yu, B. Carmichael, S.V. Kalinin, A. Tselev, Quantification of surface displacements and electromechanical phenomena via dynamic atomic force microscopy. *Nanotechnology* **27**, 425707 (2016). <https://doi.org/10.1088/0957-4484/27/42/425707>
36. D. Nečas, P. Klapetek, Gwyddion: an open-source software for SPM data analysis. *Centr. Eur. J. Phys.* **10**, 181 (2012). <https://doi.org/10.2478/s11534-011-0096-2>
37. N. Balke, S. Jesse, Q. Li, P. Maksymovych, M.B. Okatan, E. Strelcov, A. Tselev, S.V. Kalinin, Current and surface charge modified hysteresis loops in ferroelectric thin films. *J. Appl. Phys.* **118**, 072013 (2015). <https://doi.org/10.1063/1.4927811>
38. D. Seol, B. Kim, Y. Kim, Review: non-piezoelectric effects in piezoresponse force microscopy. *Current Appl. Phys.* **17**, 661 (2017). <https://doi.org/10.1016/j.cap.2016.12.012>
39. I.L. Guy, S. Muensit, E.M. Goldys, Extensional piezoelectric coefficients of gallium nitride and aluminum nitride. *Appl. Phys. Lett.* **75**, 4133–4135 (1999). <https://doi.org/10.1063/1.125560>
40. K. Lefki, G.J.M. Dormans, Measurement of piezoelectric coefficients of ferroelectric thin films. *J. Appl. Phys.* **76**, 1764 (1994). <https://doi.org/10.1063/1.357693>
41. C.M. Lueng, H.L.W. Chan, C. Surya, C.L. Choy, Piezoelectric coefficient of aluminum nitride and gallium nitride. *J. Appl. Phys.* **88**, 5360 (2000). <https://doi.org/10.1063/1.1317244>
42. R.T. Smith, F.S. Welsh, Temperature dependence of the elastic, piezoelectric, and dielectric constants of lithium

- tantalate and lithium niobate. *J. Appl. Phys.* **42**, 2219 (1971). <https://doi.org/10.1063/1.1660528>
43. X. Xu, H. Wu, C. Zhang, Z. Jin, Morphological properties of AlN piezoelectric thin films deposited by DC reactive magnetron sputtering. *Thin Solid Films* **388**, 62 (2001). [https://doi.org/10.1016/S0040-6090\(00\)01914-3](https://doi.org/10.1016/S0040-6090(00)01914-3)
44. M. Ishihara, S.J. Li, H. Yumoto, K. Akashi, Y. Ide, Control of preferential orientation of AlN films prepared by the reactive sputtering method. *Thin Solid Films* **316**, 152 (1998). [https://doi.org/10.1016/S0040-6090\(98\)00406-4](https://doi.org/10.1016/S0040-6090(98)00406-4)

**Publisher's Note** Springer Nature remains neutral with regard to jurisdictional claims in published maps and institutional affiliations.